MNRAS 000, 1–8 (2021) Preprint 7 December 2021 Compiled using MNRAS LATEX style file v3.0

An open-source Python package for modelling the vertical structure of accretion discs

A. S. Tavleev,[1]★ G. V. Lipunova,[1] and K. L. Malanchev[1]
[1] *Sternberg Astronomical Institute, Moscow M. V. Lomonosov State University, 13 Universitetski pr., Moscow, 119992, Russia*

Accepted XXX. Received YYY; in original form ZZZ

ABSTRACT

We introduce an open code, which calculates vertical structure of accretion discs around different objects (neutron stars or black holes). Code allows to use different types of equation of state and opacity laws, including tabular values. Both radiative and convection energy transport is used.

Key words: keyword1 – keyword2 – keyword3

1 INTRODUCTION

Over the past 50 years, astrophysics of accretion has been developing rapidly and fruitfully. In particular, disc accretion occurs in X-ray binaries, which are binary stars, where one of the component is either neutron star or black hole. The high luminosity of these sources is explained by the overflow of matter in the system from a companion star to a compact object. If the overflowing matter has a nonzero angular momentum, then an accretion disc is formed. For example, this happens when a neighboring star fills its Roche lobe and flows through the Lagrange point.

Due to the differential rotation of the accretion disc and viscosity, the angular momentum is transferred outward. The most likely source of viscosity is turbulent gas motions. It is convenient to characterize the efficiency of torque transfer by the α-parameter ($\alpha < 1$) (Shakura 1972). The corresponding discs are called α-discs. Shakura & Sunyaev (1973) derived the equations and analytical solutions, that describe the radial structure of an accretion α-disc.

In most cases, bursts in accretion sources are associated with a change in the accretion rate onto the central object. These changes can be associated with both variations in the rate of material supply to the disc, and with various processes caused by non-equilibrium states in the disc itself.

The accretion disc is subject to various instabilities. The main ones are the instability with respect to fluctuations in the surface density of the disc Σ_0 (viscous) and instability with respect to temperature fluctuations (thermal).

Burst model based on the study of disc instabilities is developed by a lot of authors for many years (note some: Hōshi (1979); Smak (1982a); Meyer & Meyer-Hofmeister (1981, 1982); Faulkner et al. (1983); Papaloizou et al. (1983); Smak (1984)).

At present, this model is actively developing (see. reviews Lasota 2001; Hameury 2020). It is called DIM (Disc Instability Model) (Disc Instability Model Hameury et al. 1998).

The outburst in this model is explained as follows (Frank et al. 2002; Done et al. 2007; Kato et al. 2008). A cold neutral disc is fueled by gas flowing from a companion star. When the temperature in the disc reaches values at which hydrogen ionizes, a viscous-thermal instability develops. This instability leads to an increase in the accretion rate and to the propagation of hot fronts along the disc from the inside out. After the matter falls onto a compact object, the disc begins to cool, and a cold front propagates from outside to inside. After that, the disc again passes into a cold neutral state and the process starts over.

It is convenient to study instabilities in a disc by analyzing the so-called S-curves (Meyer & Meyer-Hofmeister 1981), equilibrium curves, the middle part of which represent an unstable state of the disc. The S-curve shows schematically how the disc exhibits a ”periodic cycle” and oscillates between cold neutral and hot ionized states.

Characteristics of bursts in accretion discs can be obtained from an analysis of the structure of a quasi-stationary disc. The onset of instabilities in a disc depends on its characteristics such as surface density and temperature. Their values are determined by the specific distribution of various parameters of the disc along the vertical coordinate, that is, the vertical structure of the disc. Therefore, to study instabilities in the disc, it is necessary to solve the equations of the vertical structure. In the form of functions of dimensionless variables, the vertical structure was constructed in (Ketsaris & Shakura 1998; Malanchev et al. 2017), where analytical formulas for the opacity coefficient and the equation of state were used. In our work, we solve the same equations, but we use tabular values of opacity and equations of state and take into account the transfer of energy by convection. For this, the software package MESA (Paxton et al. 2011) is used.

In the section 2, we describe the system of equations of the vertical structure and boundary conditions, and also describe the code that numerically integrates the system. The numerical solution of the system for the power-law opacity is derived and studied in the section 3. In the section 4, the thermal and viscous balance of α-discs and its features depending on the chemical composition and the presence of convection are investigated by the method of constructing S-curves.

★ E-mail: tavleev.as15@physics.msu.ru

2 MODELLING OF ACCRETION DISC VERTICAL STRUCTURE

2.1 Vertical structure equations

Vertical structure is the dependence of various parameters on the vertical coordinate z at fixed radius r. Let's use a cylindrical coordinate system (r, φ, z), where z changes from 0 in the symmetry plane to the z_0 (the semi-thickness of disc) on the disc surface.

Let's consider geometrically thin ($z_0 \ll r$) Keplerian ($\omega = \omega_K = \sqrt{GM/r^3}$) stationary ($\partial\Sigma_0/\partial t = 0$) optically thick ($\tau \gg 1$) accretion disc.

The characteristic viscous time (time of radial structure changing) for such discs is much greater than the characteristic hydrostatic time (time of vertical structure changing):

$$t_{\rm vis} \sim \frac{r}{|v_r|} = \frac{2\pi}{\alpha\omega_K}, \quad t_{\rm hyd} \sim \frac{z_0}{v_{\rm s}} \sim \frac{1}{\omega}, \quad t_{\rm vis} \gg t_{\rm hyd}. \tag{1}$$

Therefore the vertical structure can be decoupled from radial structure.

(i) The disc is assumed to be in hydrostatic equilibrium in the vertical coordinate z:

$$\frac{{\rm d}P}{{\rm d}z} = -\rho g_z, \tag{2}$$

where $g_z = GMz/(r^2+z^2)^{3/2} \approx GMz/r^3 = \omega_K^2 z$ is the z-projection of gravitational acceleration, P and ρ are the gas pressure and bulk density. We obtain:

$$\frac{{\rm d}P}{{\rm d}z} = -\rho\,\omega_K^2 z. \tag{3}$$

(ii) Disc is heated by viscous friction between rings. Equation of viscous heating rate:

$$\frac{{\rm d}Q_{\rm vis}}{{\rm d}z} = -w_{r\varphi} r \frac{{\rm d}\omega}{{\rm d}r} = \frac{3}{2} w_{r\varphi}\omega_K, \tag{4}$$

where $w_{r\varphi}$ is the $r\varphi$-component of tensor of viscous tensions, and $Q_{\rm vis}$ is the energy flux due to viscosity. We use the α-prescription disc model (Shakura & Sunyaev 1973), where $w_{r\varphi} = \alpha P$, and α is the turbulent parameter ($0 < \alpha < 1$). Finally:

$$\frac{{\rm d}Q_{\rm vis}}{{\rm d}z} = \frac{3}{2}\omega_K \alpha P. \tag{5}$$

(iii) Disc is cooled by radiation and convection. Full energy flux consist of radiative and convective component:

$$Q^- = Q_{\rm rad} + Q_{\rm conv}, \tag{6}$$

where radiative flux is defined by temperature gradient ∇:

$$Q_{\rm rad} = \frac{4acg_z}{3\varkappa_R}\frac{T^4}{P}\nabla, \tag{7}$$

Temperature gradient defines as

$$\frac{{\rm d}\ln T}{{\rm d}\ln P} \equiv \nabla = \begin{cases} \nabla_{\rm rad}, \ \nabla_{\rm rad} < \nabla_{\rm ad}, \\ \nabla_{\rm conv}, \ \nabla_{\rm rad} > \nabla_{\rm ad}, \end{cases} \tag{8}$$

where $\nabla_{\rm rad}$ is radiative gradient, $\nabla_{\rm ad}$ is adiabatic gradient and $\nabla_{\rm conv}$ is the gradient, if both convection and radiation occur. If radiative gradient if overadiabatic, the convection takes place (Schwarzschild criteria).

Radiative gradient defines as:

$$\nabla_{\rm rad} = \frac{3\varkappa_R}{4acg_z}\frac{P}{T^4}Q^-, \tag{9}$$

where $\varkappa_R$ is he Rosseland opacity coefficient, $a = 4\sigma_{\rm SB}/c$ is the radiation constant, c is the speed of light.

Gradient in case of convection presence is calculated according to mixing length theory (see Paczyński 1969; Kippenhahn et al. 2012, for the theory description and gradient formulas). It's assumed, that convective elements have mean free path called 'mixing length', after which elements dissolve.

Theory gives the following formulas for $\nabla_{\rm conv}$:

$$\nabla_{\rm conv} = \nabla_{\rm ad} + (\nabla_{\rm rad} - \nabla_{\rm ad})Y(Y+V), \tag{10}$$

where Y is the solution of cubic equation

$$\frac{9}{4}\frac{\tau_{ml}^2}{3+\tau_{ml}^2}Y^3 + VY^2 + V^2Y - V = 0. \tag{11}$$

Here $\tau_{ml} = \varkappa\rho H_{ml}$ is the optical width of convective vortex, $H_{ml} = \alpha_{ml}H_P$ is the mixing length, $H_P = P/(\rho g_z + \omega_K\sqrt{P\rho})$ is the pressure scale height, α_{ml} coefficient is the free parameter. Usually $1 < \alpha_{ml} < 2$ for solar composition. We use $\alpha_{ml} = 1.5$, following Hameury et al. (1998). Coefficient V defines as

$$V^{-2} = -\left(\frac{3+\tau_{ml}^2}{3\tau_{ml}}\right)^2 \frac{C_P^2 H_{ml}^2 \rho^2 g_z}{512\sigma_{SB}^2 T^6 H_P}(\nabla_{\rm rad} - \nabla_{\rm ad})\left(\frac{\partial\ln\rho}{\partial\ln T}\right)_P, \tag{12}$$

where C_p is the specific heat at constant pressure.

Values of $\nabla_{\rm ad}, C_p, \left(\frac{\partial\ln\rho}{\partial\ln T}\right)_P$ are obtained from the MESA code (Paxton et al. 2011).

Finally, the temperature equation is

$$\frac{{\rm d}T}{{\rm d}z} = \nabla\frac{T}{P}\frac{{\rm d}P}{{\rm d}z}. \tag{13}$$

(iv) Surface density of disc defines as

$$\Sigma_0 = \int_{-z_0}^{+z_0}\rho(z){\rm d}z = 2\int_0^{z_0}\rho(z){\rm d}z. \tag{14}$$

Let's introduce $\Sigma(z)$ coordinate, it's the surface density "accumulated" to a certain z height. Thus the equation for Σ:

$$\frac{{\rm d}\Sigma}{{\rm d}z} = -2\rho. \tag{15}$$

Thus we obtain system of 4 ordinary differential equations (3), (5), (13), (15). System should be supplemented by equation of state (EOS) and opacity law:

$$\rho = \rho(P,T), \quad \varkappa_R = \varkappa_R(\rho,T). \tag{16}$$

Code is allow to use both analytical and tabular values of EOS and $\varkappa_R$. Characteristic values of opacities are shown on Fig. 1.

For wide range of densities and temperatures opacity coefficient can be approximated by a power-law function:

$$\varkappa_R = \varkappa_0\rho^\zeta T^\gamma, \tag{17}$$

where $\varkappa_0, \gamma, \zeta$ defines the type of opacity.

In code one can use the following options: Kramers law ($\varkappa_0 = 5\cdot 10^{24}, \zeta = 1, \gamma = -7/2$, b-b and f-f transitions in solar medium (Frank et al. 2002)) and formulas from Bell & Lin (1994): OPAL approximation ($\varkappa_0 = 1{,}5\cdot 10^{20}, \zeta = 1, \gamma = -5/2$) and hydrogen atoms scattering formula ($\varkappa_0 = 1\cdot 10^{-36}, \zeta = 1/3, \gamma = 10$).

MESA code (Paxton et al. 2011) is used to interpolate tabular values of opacity (Iglesias & Rogers 1993, 1996; Ferguson et al. 2005) and EOS (Rogers & Nayfonov 2002). Also one can use different chemical composition.

Also, system (3), (5), (13), (15) should be supplemented by the boundary conditions:

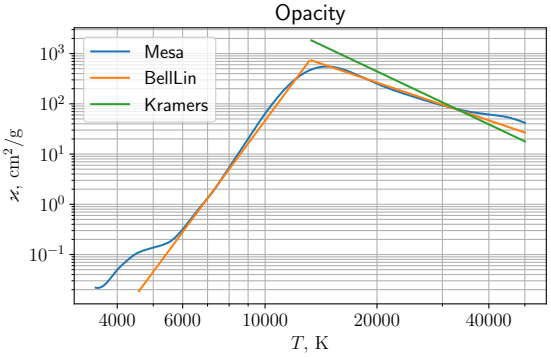

Figure 1. Opacity coefficient as function of temperature for different opacity models with $\rho = 10^{-7}$ g/cm^3). MESA code with solar chemical composition is used to interpolate tabular values.

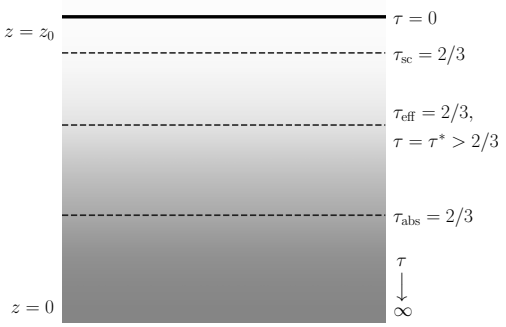

Figure 2. Optical depth τ as function of vertical coordinate in case where scattering processes are significant. Shown are effective and actual τ and τ in respect of absorption ($\tau_{\rm abs}$) and scattering ($\tau_{\rm sc}$).

(i) Full energy released from unit surface area per unit time:

$$Q_{\rm vis}(z_0) = \int_0^{z_0} \frac{{\rm d}Q_{\rm vis}}{{\rm d}z}{\rm d}z = \frac{1}{2} W_{r\varphi} r \frac{{\rm d}\omega}{{\rm d}r}, \tag{18}$$

where $W_{r\varphi} = -\int_{-z_0}^{+z_0} w_{r\varphi}{\rm d}z$.

In stationary case ($\partial\Sigma/\partial t = 0$) the accretion rate $\dot{M}$ (the mass of matter that cross the disc at radius r per unit time) is constant:

$$-2\pi r v_r \Sigma_0 = \dot{M} = {\rm const}, \tag{19}$$

The momentum conservation law gives (see Shakura et al. 2018):

$$\dot{M}(h - h_{\rm in}) = F - F_{\rm in}. \tag{20}$$

Here $F = 2\pi r^2 W_{r\varphi}$ is full viscous torque between two rings in disc, $h = \omega r^2$ is the specific angular momentum. Eq. (20) can be rewritten as:

$$W_{r\varphi} = \frac{\dot{M}\omega}{2\pi} f(r) \qquad F = \dot{M} h f(r), \tag{21}$$

where $f(r) = 1 - h_{\rm in}/h + F_{\rm in}/(\dot{M}h)$.

Finally, from (21) and (18) in Newtonian approximation ($h = \sqrt{GMr}$) for disc with $W_{r\varphi}(r_{\rm in}) = 0$ we obtain:

$$Q_{\rm vis}(z_0) = \frac{3}{8\pi}\dot{M}\omega_K^2 \left(1 - \sqrt{\frac{r_{\rm in}}{r}}\right) = \frac{3}{8\pi}\frac{F\omega_K}{r^2} = Q_0. \tag{22}$$

(ii) It's convenient to use the zero Σ boundary condition:

$$\Sigma(z_0) = 0. \tag{23}$$

(iii) To obtain the boundary condition for pressure rewrite (3) in terms of optical depth:

$${\rm d}\tau = -\varkappa_R \rho {\rm d}z. \tag{24}$$

Thus we obtain:

$$\frac{{\rm d}P}{{\rm d}\tau} = \frac{\omega_K^2 z}{\varkappa_R}. \tag{25}$$

Close to the photosphere z coordinate practically doesn't change and equal to z_0. Opacity $\varkappa_R$ is the function of bulk density and temperature. At high temperatures the scattering processes are essential. For taking into account both absorption and scattering effects the effective optical depth $\tau_{\rm eff}$ is introduced (Zel'dovich & Shakura 1969; Felten & Rees 1972; Rybicki & Lightman 1986):

$${\rm d}\tau_{\rm eff} = -\sqrt{\varkappa_{\rm abs}(\varkappa_{\rm sc} + \varkappa_{\rm abs})}\rho {\rm d}z = \sqrt{\frac{\varkappa_{\rm abs}}{\varkappa_R}}{\rm d}\tau, \tag{26}$$

where $\varkappa_{\rm abs}, \varkappa_{sc}$ are the absorption and scattering opacities respectively, $\varkappa_R \approx \varkappa_{\rm sc} + \varkappa_{\rm abs}$.

The photospherical height z_0 defines as surface, where

$$\tau_{\rm eff} = \int_0^{\tau^*} \sqrt{\frac{\varkappa_{\rm abs}}{\varkappa_R}}{\rm d}\tau = \frac{2}{3}, \tag{27}$$

Here τ^* is the full optical depth on the photospherical height. If the role of scattering is negligible, $\tau^* \approx 2/3$. Otherwise $\tau^* \gg 2/3$. Fig. 2 schematically shows all the optical depths.

Boundary condition for temperature can be found, if we use the grey Eddington approximation:

$$\frac{T}{T_{\rm eff}} = \left(\frac{1 + \frac{3}{2}\tau}{2}\right)^{1/4}, \tag{28}$$

where the effective temperature:

$$T_{\rm eff} = \left(\frac{Q_0}{\sigma_{SB}}\right)^{1/4}. \tag{29}$$

Thus

$$T(z_0) = T_{\rm eff}\left(\frac{1}{2} + \frac{3}{4}\tau^*\right)^{1/4} = T'. \tag{30}$$

If the role of scattering is small, $T' = T_{\rm eff}$, because $\tau^* \approx 2/3$. Otherwise, $T' > T_{\rm eff}$.

Integrating equation (25) with (28) gives the boundary condition for pressure:

$$P(z_0) = P' = \int_0^{\tau^*} \frac{\omega_{\rm K}^2 z_0}{\varkappa(P, T(\tau))}{\rm d}\tau \tag{31}$$

Disc is assumed to be in local thermodynamic equilibrium. The heat releases due to viscosity, i.e. the heating flux $Q^+ = Q_{\rm vis}$. Heating is compensated by radiative and convective cooling, and the cooling rate is Q^- (6). There is no advection, so $Q^+ = Q^- = Q$.

System has one free parameter z_0 — the half-thickness of the disc. To solve system one has to define the additional boundary condition at the symmetry plane of the disc ($z = 0$):

$$Q(0) = 0. \tag{32}$$

2.2 Calculation

Thus the system consists of 4 equations (3), (5), (13), (15) with 4 boundary conditions (22), (23), (31), (30) and with additional

boundary condition (32) and one free parameter z_0. This system can be solved using so-called shooting method.

By normalizing P, Q, T, Σ on their characteristic values P_0, Q_0, T_0, Σ_{00}, and replacing z on $\hat{z} = 1 - z/z_0$, we obtain the final system:

$$\begin{aligned}
\frac{\mathrm{d}\hat{P}}{\mathrm{d}\hat{z}} &= \frac{z_0^2}{P_0}\,\omega_K^2\,\rho(1-\hat{z}) && \hat{P}(0) = P'/P_0,\\
\frac{\mathrm{d}\hat{\Sigma}}{\mathrm{d}\hat{z}} &= 2\,\frac{z_0}{\Sigma_{00}}\,\rho, && \hat{\Sigma}(0) = 0,\\
\frac{\mathrm{d}\hat{T}}{\mathrm{d}\hat{z}} &= \nabla\frac{\hat{T}}{\hat{P}}\frac{\mathrm{d}\hat{P}}{\mathrm{d}\hat{z}}, && \hat{T}(0) = T'/T_0,\\
\frac{\mathrm{d}\hat{Q}}{\mathrm{d}\hat{z}} &= -\frac{3}{2}\,\frac{z_0 P_0}{Q_0}\,\omega_K\,\alpha\hat{P} && \hat{Q}(0) = 1, \quad \hat{Q}(1) = 0,
\end{aligned} \tag{33}$$

where $\hat{P}$, $\hat{\Sigma}$, $\hat{T}$, $\hat{Q}$ are dimensionless functions of $\hat{z}$. Note, that ∇ is the temperature gradient (13).

System (33) was solved in Ketsaris & Shakura (1998) in case of analytical opacities and ideal gas EOS. They use Kramers formula for opacity in absorption regions and Thomson scattering formula in regions, where scattering is dominated. System was solved using so-called dimensionless Π-parameters:

$$\begin{aligned}
\Pi_1 &= \frac{\omega_K^2\, z_0^2\, \rho_c}{P_c}, && \Pi_2 = \frac{\Sigma_0}{2 z_0\, \rho_c},\\
\Pi_3 &= \frac{3}{4}\,\frac{\alpha\,\omega_K\, P_c\, \Sigma_0}{\rho_c Q_0}, && \Pi_4 = \frac{3}{32}\left(\frac{T_{\mathrm{eff}}}{T_c}\right)^4 \Sigma_0\,\varkappa_c.
\end{aligned} \tag{34}$$

Here P_c, T_c, ρ_c are the pressure, temperature and bulk density in the symmetry plane of the disc.

Characteristic values of pressure, temperature and mass coordinate (T_0, P_0, Σ_{00}) can be obtained by equating $\Pi_1 = 1$, $\Pi_2 = 7/2$, $\Pi_3 = 7$:

$$T_0 = \frac{\mu}{\mathcal{R}}\omega_K^2 z_0^2, \quad P_0 = \frac{4}{3}\,\frac{Q_0}{\alpha z_0 \omega_K}, \quad \Sigma_{00} = \frac{28}{3}\,\frac{Q_0}{\alpha z_0^2 \omega_K^3} \tag{35}$$

The input parameters of system: mass of central object M, radius r, the viscous torque F (or accretion rate $\dot{M}$, or effective temperature T_{eff}), type of opacity (Kramers, BellLin or MESA) and EOS (ideal gas with molecular weight μ or MESA), turbulence parameter α. Note, that surface density of disc $\Sigma_0 = \hat{\Sigma}(1) \cdot \Sigma_{00}$.

Python 3 code solve the optimization problem and finds the free parameter z_0 using shooting method. Scipy (Jones et al. 2019), Numpy (Walt et al. 2011), Matplotlib (Hunter 2007) and Astropy (Astropy Collaboration et al. 2013, 2018) packages are used in code.

Fig. 3 shows examples of vertical structure for different disc states. Shown are temperature as function of z for cold disc, hot disc and unstable disc with different chemical composition. Adiabatic and actual temperature gradients and ionisation parameters are also shown. Note, that ionisation parameter (equaled $1/\mu_e$) is the mean number of free electrons per nucleon. It can change from 0 in neutral matter to $(1 + X)/2$ (X is hydrogen abundance) in fully ionized matter.

3 RADIAL STRUCTURE OF SOLAR DISCS

Usually accretion disc is divided into 3 zones. In zone A, the radiation pressure is greater than the gas pressure, and opacity as determined by scattering processes. In zone B, the gas pressure is greater than the radiation pressure, but opacity is still determined by scattering. Finally, in zone C, opacity is determined by the absorption processes, and gas pressure is much greater than the radiation pressure.

Using the obtained solutions of the vertical structure, one can obtain analytical formulas for the radial distribution of z_0/r, Σ_0, T_c, ρ_c in the C zone of the disc. For Kramers opacity law, such dependencies were obtained earlier (see, e.g., Shakura et al. 2018, chapter 1). Since the tabular opacity for the solar chemical composition is better approximated by a formula with another power-law dependences (see (17)), the result for the radial structure will have a slightly different form. Let us substitute the analytical equations of state and the opacity law into the definitions of Π-parameters. We will use the ideal gas equation of state and the opacity approximation formula obtained by the OPAL project:

$$P_c = \frac{\rho_c \mathcal{R} T_c}{\mu} \qquad \varkappa_c = \varkappa_0 \frac{\rho_c}{T_c^{5/2}},\ \varkappa_0 = 1.5 \cdot 10^{20} \mathrm{cm}^5\,\mathrm{K}^{5/2}\,\mathrm{g}^{-2}. \tag{36}$$

Solving algebraic equations (34) for $\Pi_{1..4}$ with (36), we obtain:

$$\begin{aligned}
z_0/r &= 0.021\, m^{-13/36} \alpha^{-1/9}\, r_{10}^{1/12}\, \dot{M}_{17}^{1/6}\, f(r)^{1/6} \left(\frac{\mu}{0.6}\right)^{-13/36} \left(\frac{\varkappa_0}{\varkappa_0^*}\right)^{1/18} \Pi_z,\\
\Sigma_0 &= 32\, m^{2/9}\, \alpha^{-7/9}\, r_{10}^{-2/3}\, \dot{M}_{17}^{2/3}\, f(r)^{2/3} \left(\frac{\mu}{0.6}\right)^{13/18} \left(\frac{\varkappa_0}{\varkappa_0^*}\right)^{-1/9} \Pi_\Sigma\ [\mathrm{g/cm^2}],\\
\rho_c &= 7.8 \cdot 10^{-8}\, m^{7/12}\, \alpha^{-2/3}\, r_{10}^{-7/4}\, \dot{M}_{17}^{1/2}\, f(r)^{1/2} \left(\frac{\mu}{0.6}\right)^{13/12} \left(\frac{\varkappa_0}{\varkappa_0^*}\right)^{-1/6} \Pi_\rho\ [\mathrm{g/c}\\
T_c &= 4.1 \cdot 10^4\, m^{5/18}\, \alpha^{-2/9}\, r_{10}^{-5/6}\, \dot{M}_{17}^{1/3}\, f(r)^{1/3} \left(\frac{\mu}{0.6}\right)^{5/18} \left(\frac{\varkappa_0}{\varkappa_0^*}\right)^{1/9} \Pi_T\ [\mathrm{K}].
\end{aligned} \tag{37}$$

Here:

$$\begin{aligned}
&m = \frac{M}{M_\odot} \quad \dot{M}_{17} = \frac{\dot{M}}{10^{17}\ \mathrm{g/s}} \quad r_{10} = \frac{r}{10^{10}\ \mathrm{cm}}\\
&\varkappa_0^* = 1.5 \cdot 10^{20}\ \mathrm{cm}^5\mathrm{g}^{-2}\mathrm{K}^{5/2}.
\end{aligned} \tag{38}$$

Dimensionless parameters $\Pi_z, \Pi_\Sigma, \Pi_\rho, \Pi_T$ defines as follows:

$$\begin{aligned}
\Pi_z &= \Pi_1^{17/36}\, \Pi_2^{-1/18}\, \Pi_3^{1/9}\, \Pi_4^{-1/18} \approx 2.52,\\
\Pi_\Sigma &= \Pi_1^{1/18}\, \Pi_2^{1/9}\, \Pi_3^{7/9}\, \Pi_4^{1/9} \approx 1.05,\\
\Pi_\rho &= \Pi_1^{-5/12}\, \Pi_2^{-5/6}\, \Pi_3^{2/3}\, \Pi_4^{1/6} \approx 0.771,\\
\Pi_T &= \Pi_1^{-1/18}\, \Pi_2^{-1/9}\, \Pi_3^{2/9}\, \Pi_4^{-1/9} \approx 1.095.
\end{aligned} \tag{39}$$

Boundary between B zone and C zone can be obtained from the equality of electron scattering $\varkappa_T$ and absorption $\varkappa_{\mathrm{ff}} = \varkappa_0 \rho_c T_c^{-5/2}$ opacity coefficients:

$$R_{BC} \sim 6.8{\cdot}10^4\, m^{1/3}\, \alpha^{1/3}\, \dot{M}_{17}\, f(r) \left(\frac{\mu}{0.6}\right)^{-7/6} \left(\frac{\varkappa_0}{\varkappa_0^*}\right)^{-5/3} \left(\frac{\varkappa_T}{\varkappa_T^*}\right)^3 \mathrm{cm}, \tag{40}$$

where $\varkappa_T^* = 0.4\,\mathrm{cm}^2/\mathrm{g}$.

Boundary between A zone and B zone, R_{AB}, can be obtained from the equality of P_{rad} and P_{gas}, while opacity is determined by scattering:

$$R_{AB} \sim 10^7\, m^{1/3}\, \alpha^{2/21}\, \dot{M}_{17}^{16/21}\, f(r)^{16/21} \left(\frac{\mu}{0.6}\right)^{8/21} \left(\frac{\varkappa_T}{\varkappa_T^*}\right)^{6/7} \mathrm{cm}. \tag{41}$$

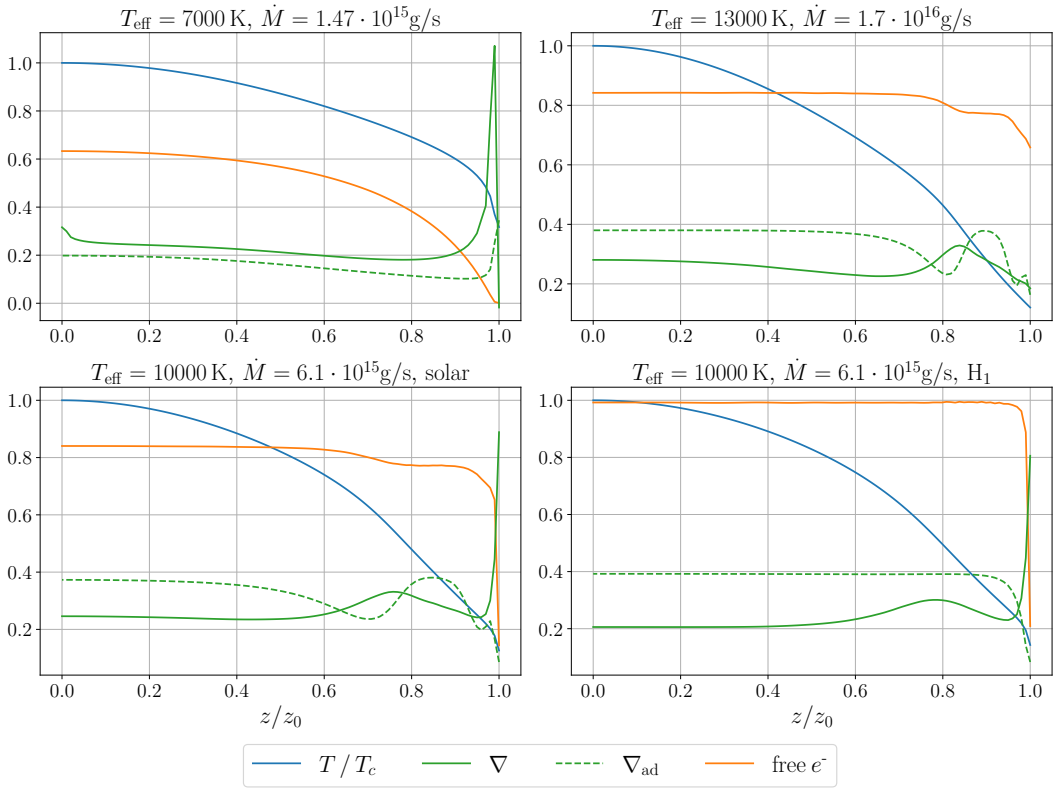

Figure 3. Vertical structures for $M = 6M_\odot$, $\alpha = 0.01$, $r = 10^{10}$ cm and tabular opacity. Shown are temperature T, temperature gradient ∇, adiabatic gradient $\nabla_{\rm ad}$ and ionization parameter. Upper figures are calculated for cold ($T_{\rm eff} = 7000\,{\rm K}$) and hot discs ($T_{\rm eff} = 13000\,{\rm K}$) with solar composition. Lower figures are calculated for unstable disc with solar and hydrogen composition. One can see the absence of convection in the hot disc ($\nabla < \nabla_{\rm ad}$). Otherwise, cold neutral and unstable disc is convective.

Fig. 4 shows gas pressure to radiation pressure ratio $P_{\rm rad}/P_{\rm gas}$ and (tabular) opacity $\varkappa_c$ at the symmetry plane of the disc. To the left of the solid black vertical line, the radiation pressure prevails in the disc. The estimate of this radius from analytical opacity, namely the radius R_{AB} (41), is shown by the vertical dashed line. One can see that for central objects of both stellar masses and supermassive and for big $\dot{M}$ (about Eddington limit), the analytical estimate R_{AB} and the actual boundary of zone A are in good agreement.

The red solid line in Fig. 4 shows the radius, where the absorption opacity is equal to the scattering opacity. It can be seen that the analytical estimate of the radius of this transition R_{BC} (40) shown by the dotted line is very different from the actual value. Moreover, for $10\,M_\odot$ the actual boundaries of A and B zones are reversed, i.e. there is no B zone and there is no pure A zone (because the opacity near the edge of A zone is determined by absorption processes, not by scattering).

For $M = 10^8\,M_\odot$ in the shown range of radii, the opacity is always greater than Thomson's and is determined by absorption processes, and, in fact, there is no zone B. In addition, theoretical estimates of the boundaries of zones A and B are reversed, $R_{BC} < R_{AB}$. (Also for $M = 10^8\,M_\odot$ the hydrogen recombination zone, where the opacity decreases, is visible.)

It can be concluded that the classical division of the disc into zones A, B and C is rather approximate, and for discs around supermassive black holes it does not make sense at all.

4 DISC INSTABILITIES AND S-CURVES

As noted in the Introduction, accretion discs can be viscously and thermally unstable. In the Meyer & Meyer-Hofmeister (1981), the authors proposed to use the analysis of dependences $F - \Sigma_0$ (so-called S-curves) to study disc instability and showed that the branch of the S-curve with a negative slope is unstable with time of the order of viscous time. Smak (1984) showed that if the parameters of the disc at some radius lies on the viscous-unstable branch of the S-curve with a negative slope, then thermal instability also develops at this radius.

Note that since the stationary discs has an unambiguous relation between $F, \dot{M}$ and $T_{\rm eff}$ (see boundary conditions for flux and temperature), the S-curve can be drawn also in coordinates $\dot{M} - \Sigma_0$ and $T_{\rm eff} - \Sigma_0$.

In discs around stellar-mass black holes, ionization-thermal instability develops at low temperatures, when hydrogen is partially ionized. The vertical structure of the disc can quickly (during the thermal time) rebuild: the disc "jumps" from the lower branch of the S-curve (cold neutral disc) to the upper (hot disc) or vice versa. That is, the efficiency of energy release changes sharply when the surface density reaches critical values, corresponding to the turns on the S-curve. An example of an S-curve calculated by our code is shown in Fig. 5. The right figure shows the dependence of the opacity and the ionization parameter on the temperature at different depths z. The ionization in the center of the disc starts at a temperature of $T_c \approx 10^4$K. When ionization reaches the value of ~ 0.3, the

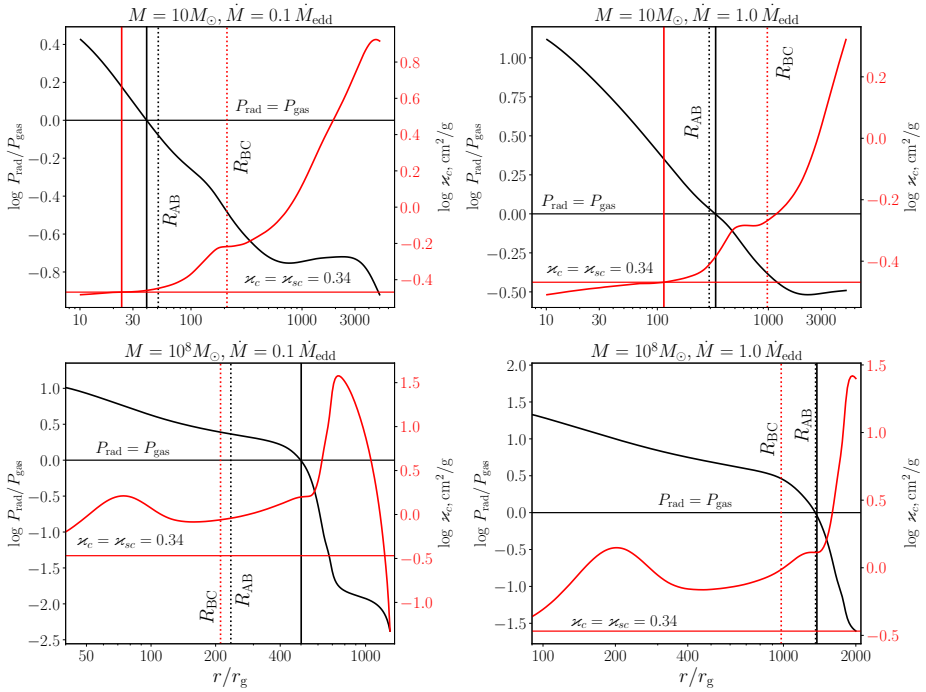

Figure 4. Ratio of radiation to gas pressure (along the left vertical axis) and opacity at the symmetry plane of the disc (along the right vertical axis) for different masses of central object and accretion rates. The black solid vertical lines show the outer boundary of the "A zone", which is dominated by the radiation pressure. For $M = 10\,M_\odot$, the red solid vertical line shows the outer boundary of the "B zone", where the opacity is equal to Thomson's. Vertical dotted lines show theoretical estimates (**??**) of the boundaries of zones A and B. Turbulence parameter $\alpha = 0.5$.

instability starts. It ends when the disc is almost completely ionized (ionization at the center is ~ 0.75).

4.1 Influence of chemical composition, α parameter, and convection on the shape of S-curve in X-ray transients

Fig. 6 and 7 show S-curves for different chemical composition and α parameter. Curves with and without convection are also shown. The dots mark the regions where convection in the disc dominates (i.e. the condition for the existence of convection $\nabla_{\rm rad} > \nabla_{\rm ad}$ is fulfilled over an z-range of more than 50%). It is seen that the disc is convective in the unstable region.

It can be seen that when convection is off (when there is only a radiative temperature gradient) there is one unstable region, regardless of the chemical composition and α. This is consistent with Faulkner et al. (1983) — convection doesn't affect the very existence of instability.

When convection is taken into account, the situation changes, instability starts at higher accretion rates. For large α, regions with convection are "pulled away" towards large Σ, an almost vertical branch is formed. For small α, the convective branch splits into two unstable branches. In this case, the upper unstable branch is associated with a peak in opacity, on which hydrogen is partially ionized. The lower branch is associated with convection (Cannizzo 1992) and with the formation of molecular hydrogen (Smak 1982b), see small peak in opacity (Fig. 1) at $T \approx 4000$ K. At large α, the lower unstable branch doesn't appear, since the temperature does not reach such low values, at which the formation of molecules begins. On the helium curve, at both large and small α, the second unstable branch doesn't appear, only the main unstable branch is deformed.

These results are consistent with the results in Cannizzo et al. (1982), where S-curves were investigated taking into account convection, which led to the appearance of additional kinks on the curve.

5 DISCUSSION

6 CONCLUSIONS

ACKNOWLEDGEMENTS

The work was supported by the RSF grant 21-12-00141.

DATA AVAILABILITY

The inclusion of a Data Availability Statement is a requirement for articles published in MNRAS. Data Availability Statements provide a standardised format for readers to understand the availability of data underlying the research results described in the article. The statement may refer to original data generated in the course of the study or to third-party data analysed in the article. The statement should describe and provide means of access, where possible, by linking to the data or providing the required accession numbers for the relevant databases or DOIs.

REFERENCES

Astropy Collaboration et al., 2013, A&A, 558, A33
Astropy Collaboration et al., 2018, AJ, 156, 123
Bell K. R., Lin D. N. C., 1994, ApJ, 427, 987
Cannizzo J. K., 1992, ApJ, 385, 94
Cannizzo J. K., Ghosh P., Wheeler J. C., 1982, ApJ, 260, L83
Done C., Gierliński M., Kubota A., 2007, A&ARv, 15, 1

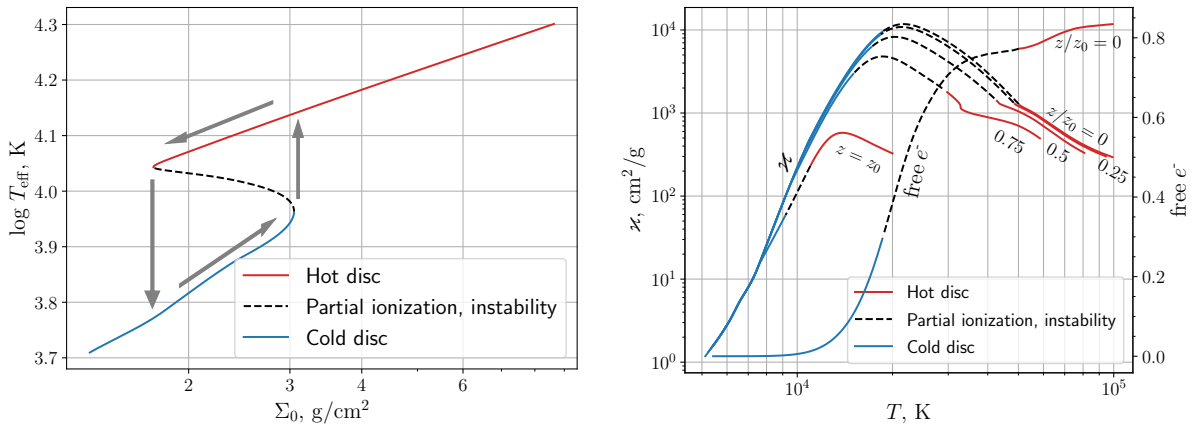

Figure 5. On the left side shown is the S-curve obtained for $M = 6M_\odot$, $\alpha = 0.01$, $r = 1.8 \cdot 10^8$ cm and tabular opacities with solar chemical composition. Also the limit cycle instability is showed by arrows. On the right side shown is the opacity coefficient as a function of temperature for the same parameters at different depths (at $z/z_0 = 0,\ 0.25,\ 0.5,\ 0.75$). Shown also the dependence of the ionization parameter on temperature at the symmetry plane of the disc. The cold disc region, the region of partial ionization (in which the instability takes place) and the region of the hot disc are marked by different styles. In the unstable region, the ionization parameter at the center changes from 0.3 to 0.77 (full ionization in the hot disc corresponds to a parameter equal to 0.85).

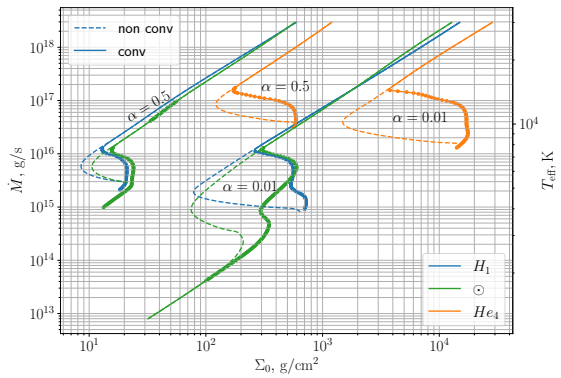

Figure 6. S-curves for different chemical composition, α, with and without convection. All curves are calculated for $M = M_\odot$ and $r = 10^{10}$ cm. Bold point regions are the zones where the disc is convective (i.e. the condition for the existence of convection $\nabla_{\rm rad} > \nabla_{\rm ad}$ is fulfilled over an z-range of more than 50%). Note that only the optically thick branches of the curves are shown. For this reason, the curves for the helium and hydrogen disc do not show the area corresponding to the cold disc, since it's optically thin.

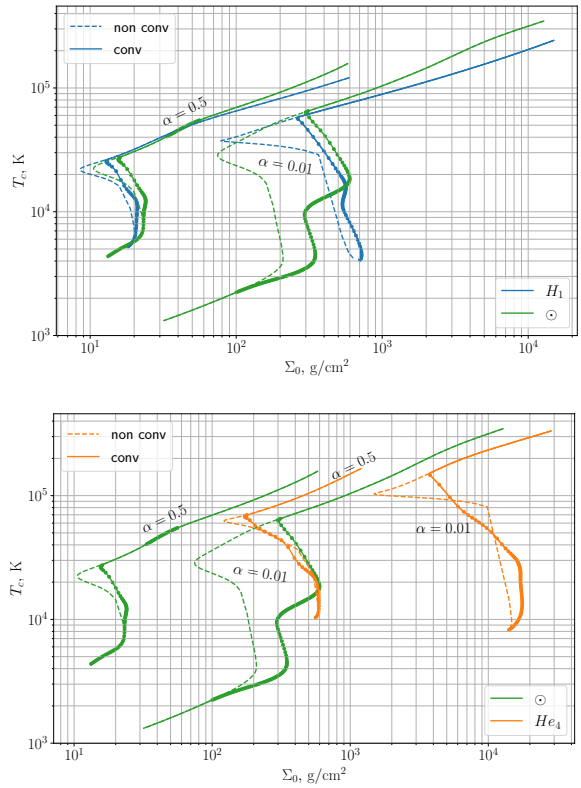

Figure 7. $T_c - \Sigma_0$ dependencies for different chemical composition, α, with and without convection. System parameters and notations are the same as in Fig. 6.

Faulkner J., Lin D. N. C., Papaloizou J., 1983, MNRAS, 205, 359
Felten J. E., Rees M. J., 1972, A&A, 17, 226
Ferguson J. W., Alexander D. R., Allard F., et al., 2005, ApJ, 623, 585
Frank J., King A., Raine D. J., 2002, Accretion Power in Astrophysics: Third Edition
Hameury J. M., 2020, Advances in Space Research, 66, 1004
Hameury J.-M., Menou K., Dubus G., et al., 1998, MNRAS, 298, 1048
Hōshi R., 1979, Progress of Theoretical Physics, 61, 1307
Hunter J. D., 2007, Computing in Science & Engineering, 9, 90
Iglesias C. A., Rogers F. J., 1993, ApJ, 412, 752
Iglesias C. A., Rogers F. J., 1996, ApJ, 464, 943
Jones E., Oliphant T., Peterson P., et al., 2001–2019, SciPy: Open source scientific tools for Python, `http://www.scipy.org/`
Kato S., Fukue J., Mineshige S., 2008, Black-Hole Accretion Disks — Towards a New Paradigm —
Ketsaris N. A., Shakura N. I., 1998, Astronomical and Astrophysical Transactions, 15, 193
Kippenhahn R., Weigert A., Weiss A., 2012, Stellar Structure and Evolution, doi:10.1007/978-3-642-30304-3.
Lasota J.-P., 2001, New Astron. Rev., 45, 449
Malanchev K. L., Postnov K. A., Shakura N. I., 2017, MNRAS, 464, 410
Meyer F., Meyer-Hofmeister E., 1981, A&A, 104, L10
Meyer F., Meyer-Hofmeister E., 1982, A&A, 106, 34
Paczyński B., 1969, Acta Astron., 19, 1
Papaloizou J., Faulkner J., Lin D. N. C., 1983, MNRAS, 205, 487
Paxton B., Bildsten L., Dotter A., et al., 2011, ApJS, 192, 3
Rogers F. J., Nayfonov A., 2002, ApJ, 576, 1064

Rybicki G. B., Lightman A. P., 1986, Radiative Processes in Astrophysics
Shakura N. I., 1972, Azh, 49, 921
Shakura N. I., Sunyaev R. A., 1973, A&A, 500, 33
Shakura N. I., Lipunova G. V., Malanchev K. L., et al., 2018, Accretion flows in astrophysics. New York, New York, doi:10.1007/978-3-319-93009-1
Smak J., 1982a, Acta Astron., 32, 199
Smak J., 1982b, Commmunications of the Konkoly Observatory Hungary, 83, 195
Smak J., 1984, Acta Astron., 34, 161
Walt S. v. d., Colbert S. C., Varoquaux G., 2011, Computing in Science & Engineering, 13, 22
Zel'dovich Y. B., Shakura N. I., 1969, Soviet Ast., 13, 175

This paper has been typeset from a TEX/LATEX file prepared by the author.